Image Classification Using Novel Set of Charlier Moment Invariants

Abdeslam Hmimid[1], Mhamed Sayyouri[1] and Hassan[1]
[1]CED-ST; LESSI; Faculty of sciences Dhar el mehraz
University Sidi Mohamed Ben Abdellah
BP 1796 Fez-Atlas 30003
Fez Morocco
abdeslam_ph@yahoo.fr ; mhamedsay@yahoo.fr ; qjidah@yahoo.fr

Abstract: - The use of the discrete orthogonal moments, as feature descriptors in image analysis and pattern recognition is limited by their high computational cost. To solve this problem, we propose, in this paper a new approach for fast computation of Charlier's discrete orthogonal moments. This approach is based on the use of recurrence relation with respect to variable x instead of order n in the computation of Charlier's discrete orthogonal polynomials and on the image block representation for binary images and intensity slice representation for gray-scale images. The acceleration of the computation time of Charlier moments is due to an innovative image representation, where the image is described by a number of homogenous rectangular blocks instead of individual pixels. A novel set of invariants moment based on the Charlier moments is also proposed. These invariants moment are derived algebraically from the geometric moment invariants and their computation is accelerated using image representation scheme. The proposed algorithms are tested in several well known computer vision datasets, regarding computational time, image reconstruction, invariability and classification. The performance of Charlier invariants moment used as pattern features for a pattern recognition and classification is compared with Hu and Legendre invariants moment.

Key-Words: - Charlier discrete orthogonal polynomials, Charlier moments, Charlier invariant moments, Image block representation, image slice representation, Fast computation, Image reconstruction, Pattern recognition, classification

1 Introduction

The image moments has been widely used for image analysis and pattern recognition [1]-[7]. Hu [1] is the first who introduced the geometric moments in the field of the image in 1962. He derived a full set of geometric moment invariants under translation, scaling and rotation. These invariant moments are successfully used as image descriptors in many pattern recognition and classification. However, the non orthogonal of the Geometric moments causes the redundancy of information which less efficient in difficult problems where more discriminative information needs to be captured. To overcome this problem, Teague [4] in 1980 introduced the orthogonal continuous moments defined in terms of Legendre and Zernike orthogonal continuous polynomials. The orthogonal property assures the robustness against noise and eliminates the redundancy of information [4]. The computation of continuous orthogonal moments as Legendre, Zernike, Pseudo-Zernike and Fourier-Mellin requires the discretization of continuous space and the approximation of the integral. This increases the computational complexity and causes the discretization error [5]-[9]. To eliminate this error and to simplify the computational complexity, the discrete orthogonal moments such as Tchebichef, Krawchouk, and Hahn have been introduced in image analysis and pattern recognition [10]-[13]. The discrete orthogonal moments are defined from the discrete orthogonal polynomials which eliminate the need for numerical approximation and satisfy the orthogonal property precisely [14]. Indeed, it was proved that these discrete orthogonal moments have better capability in image representation than the continuous orthogonal moments [10]-[14]. The computation of discrete orthogonal moments is limited by two major difficulties. The first is related to the high computational cost especially for large size image and the higher orders. The second is related to the propagation of numerical error in the computation of discrete orthogonal polynomials. Indeed, the calculated values of discrete orthogonal polynomials, using the hypergeometric function and recurrence relation of three-terms with respect to the order n of discrete orthogonal polynomials, are complex and require a lot of time for all higher orders which causes the propagation of numerical error [14]. To limit this error and to reduce the time calculation of moments and also to ameliorate the

accuracy of image reconstruction the scientists propose the use of the recurrence relation with respect to the variable x instead of the order n in the calculation of discrete orthogonal polynomials [13]-[14]. To reduce the computational time cost of moments, several algorithms are introduced in literature [15]-[24]. Spiliotis and Mertzios [15] have presented a fast algorithm to calculate the geometric moments for binary images using the image block representation. Papakostas et al [16] have given an algorithm that permits the fast and accurate computation of Legendre moments based on the Image Slice Representation (ISR) method. Shu et al [17] have introduced an approach to accelerate the time computation of Tchebichef moments by deriving some properties of Tchebichef polynomials and by using the image block representation for binary images and image slice representation for gray-scale images. Hosny in [20] has proposed an exact and a fast computation of geometric moments for gray scale images by applying the methodology of image block representation. The geometric invariant moments and the orthogonal invariant moments have been studied by several researchers [1]-[3], [25]-[30]. In literature, the orthogonal invariant moments are calculated directly from the orthogonal polynomials or indirectly as linear combination of geometric moments. Indeed, Chong et al [25]-[26] have introduced an effective method to construct the translation and scale invariants of Legendre and Zernike moments. Zhu and al [27] have proposed a directly method based on Tchebichef polynomials to make the translation and scale of Tchebichef invariant moments. Papakostas in [28] have introduced a set of Krawchouk invariant moments computed over a finite number of image intensity slices extracted by applying the image slice representation. Karakasis et al [30] have proposed a generalized expression of the weighted dual Hahn invariant moments up to any order and for any value of their parameters based a linear combination of geometric moments. If most work has focused on the moments of Tchebichef, Krawchouk and dual Hahn, no attention has been paid to accelerate the time computation of Charlier discrete orthogonal moments and no report has been published on how to make the translation, scale and rotation invariants of Charlier's discrete orthogonal moments. In this paper, another new set of discrete orthogonal moments called Charlier moments is proposed. It is based on the Charlier discrete orthonormal polynomials. We also propose a new algorithm to accelerate the time computation of Charlier moments. Indeed, we proposed a fast method for calculating Charlier discrete orthogonal polynomials based on the recurrence relation with respect to variable x instead of order n. Furthermore, we propose a new computation method of Charlier moments by describing an image with a set of blocks instead of individual pixels. Two algorithms of image block representation IBR for binary images and image slice representation ISR for gray-scale images are proposed. This proposed approach also discusses the ability of Charlier's discrete orthogonal moments to reconstruct binary and gray-scale images with and without noise. For the purpose of object classification, it is vital that Charlier moments be independent of rotation, scale, and translation of the image. For this, we have proposed a new set of Charlier invariant moments under translation, scaling and rotation of the image. The Charlier's invariant moments are derived algebraically from the geometric invariant moments. A fast computation algorithm of Charlier invariant moments is proposed using the image block representation. The accuracy of object classification by Charlier invariant moments is compared with Hu [1] and Legendre [31] invariant moments. The rest of the paper is organized as follows: In Section 2, we present the definition of Charlier's discrete orthogonal polynomials. Section 3 presents a fast method to calculate Charlier's moments for binary and gray-scale images. In Section 4, the reconstruction of images by Charlier moments are provided. Section 5 gives two methods to calculate Charlier's invariant moments. Section 6 provides some experimental results concerning the reduction of the time computation of Charlier's moments, the reconstruction of image and the classification of the objects. Section 7, finally concludes this work.

2 Charlier polynomials

This section aims to present a short introduction to the theoretical background of Charlier polynomials with one variable. The nth discrete orthogonal polynomials of Charlier $C_n^{a_1}(x)$ are defined by using hyper-geometric function as [32]

$$C_n^{a_1}(x) = {}_2F_0(-n,-x;;1/a_1) = \sum_{k=0}^{n} \alpha_{k,n}^{a_1} x^k \tag{1}$$

where $x, n = 0,1,2\ldots..N\text{-}1$; $a_1 > 0$

The hyper-geometric function ${}_2F_0$ is defined as

$${}_2F_1(a,b;-;x) = \sum_{k=0}^{\infty} (a)_k (b)_k \frac{x^k}{k!} \tag{2}$$

The Pochhammer symbol $(x)_k$ is defined as

$$(x)_0 = 1 \text{ and } (x)_k = x(x+1)...(x+k-1) \; ; \mathrm{k} \geq 1 \tag{3}$$

More explicitly, the nth order of Charlier discrete orthogonal polynomials defined in Eq. (1) can be rewrite as follows

$$C_n^{a_1}(x) = \sum_{k=0}^{n} \frac{(-n)_k}{(a_1)^k k!}(-x)_k \tag{4}$$

The set of Charlier polynomials $\{C_n^{a_1}(x)\}$ forms a complete set of discrete basis functions with weight function

$$w(x) = \frac{e^{-a_1} a_1^x}{x!} \tag{5}$$

and satisfies the orthogonality condition

$$\sum_{x=0}^{N} w(x) C_n^{a_1}(x) C_m^{a_1}(x) = \rho(n)\delta_{nm} \tag{6}$$

where

$$\rho(\mathrm{n}) = \frac{n!}{a_1^n} \tag{7}$$

To avoid fluctuations in the numerical calculation of Charlier orthogonal polynomials we use their normalized form. The normalized Charlier polynomials are defined as

$$\tilde{C}_n^{a_1}(x) = C_n^{a_1}(x)\sqrt{\frac{w(x)}{\rho(n)}} \tag{8}$$

In addition, to accelerate the computation of weight function and squared norm functions, we use the following recurrence relations.The weight function as given in Eq.(5) can be written by recurrence formula as

$$w(x+1) = \frac{a_1}{x+1} w(x) \qquad with \qquad w(0) = e^{-a_1} \tag{9}$$

The squared norm as given in Eq. (7) can be written by recurrence formula as

$$\rho(\mathrm{n+1}) = \frac{n+1}{a_1}\rho(\mathrm{n}) \qquad \text{with} \qquad \rho(0) = 1 \tag{10}$$

2.1 Computation of Charlier discrete orthogonal polynomials

This section discusses the computational aspects of Charlier discrete orthogonal polynomials. It is shown in the first subsection the recurrence relations used to calculate the discrete orthogonal polynomials of Charlier with respect to n. In the next subsection, the utilization of the recurrence relations with respect to variable x is shown to accelerate the computational time.

2.1.1 Recurrence relation with respect to n

As the computation of normalized Charlier polynomials by Eq. (1) has a great computational time cost, we use the following three-term recurrence relations with respect to order n [33]

$$\tilde{C}_n^{a_1}(x) = \frac{a_1 - x + n - 1}{a_1}\sqrt{\frac{a_1}{n}}\tilde{C}_{n-1}^{a_1}(x) - \sqrt{\frac{n-1}{n}}\tilde{C}_{n-2}^{a_1}(x) \tag{11}$$

The initial values of this recurrence relation are defined as

$$\tilde{C}_0^{a_1}(x) = \sqrt{\frac{w(x)}{\rho(0)}} \quad \text{and} \quad \tilde{C}_1^{a_1}(x) = \frac{a_1 - x}{a_1}\sqrt{\frac{w(x)}{\rho(1)}} \tag{12}$$

2.1.2 Recurrence relation with respect to x

In order to extract the recurrence formula with respect to variable x we will use the partial difference equation and the forward and backward finite difference operator. The discrete orthogonal polynomials of Charlier $C_n^{a_1}(x)$ satisfy the following first-order partial difference equation [32].

$$\sigma(x)\Delta\nabla\tilde{C}_n^{a_1}(x) + \tau(x)\Delta\tilde{C}_n^{a_1}(x) + \lambda_n\tilde{C}_n^{a_1}(x) = 0 \tag{13}$$

where $\sigma(x)$ and $\tau(x)$ are the second and first degree functions, respectively, λ_n is an appropriate constant defined as:

$$\sigma(x) = x \quad ; \; \tau(x) = a_1 - x \; ; \quad \lambda_n = n \tag{14}$$

The forward and backward finite difference operator Δ and ∇ are defined by:

$$\Delta P_n(x) = P_n(x+1) - P_n(x) \quad and \quad \nabla P_n(x) = P_n(x) - P_n(x-1) \tag{15}$$

Considering the properties of the operator Δ and ∇ we have

$$\Delta\nabla P_n(x) = P_n(x+1) - 2P_n(x) + P_n(x-1) \tag{16}$$

The recurrence relations of Charlier discrete orthogonal polynomials with respect to x can be obtained through Eq. (13), Eq. (15) and Eq. (16) as follows

$$\tilde{C}_1^{a_1}(x) = \frac{\sqrt{w(x)}}{\sigma(x-1)+\tau(x-1)} \times \left[\frac{2\sigma(x-1)+\tau(x-1)-\lambda_n}{\sqrt{w(x-1)}}\tilde{C}_1^{a_1}(x-1) - \frac{\sigma(x-1)+\tau(x-1)}{\sqrt{w(x-2)}}\tilde{C}_1^{a_1}(x-2)\right] \tag{17}$$

The initial values of recurrence relation with respect to x are defined as

$$\tilde{C}_n^{a_1}(0)=\sqrt{\frac{w(0)}{\rho(n)}} \quad \text{and} \quad \tilde{C}_n^{a_1}(1)=\frac{a_1-n}{a_1}\sqrt{\frac{w(1)}{w(0)}}\tilde{C}_n^{a_1}(0) \tag{18}$$

3 Fast Computation of Charlier Discrete Orthogonal Moments

The two-dimensional (2-D) Charlier discrete orthogonal moment of order (n+m) of an image intensity function $f(x,y)$ with size MxN is defined as

$$CM_{nm}=\sum_{x=0}^{M-1}\sum_{y=0}^{N-1}\tilde{C}_n^{a_1}(x)\tilde{C}_m^{a_1}(y)f(x,y) \tag{19}$$

with $\tilde{C}_n^{a_1}(x)$ is the nth order orthonormal Charlier polynomials.

The computation of Charlier moments by using Eq. (19) seems to be a time consuming task mainly due to two factors. First, the need of computing a set of complicated quantities for each moment order and second, the need to evaluate the polynomial values for each pixel of the image, decelerate the whole process. While, in the first case a recurrence relation with respect to x introduce efficient algorithm, which recursively compute the orthogonal polynomials, little attention has been given in the second case. Moreover, the computation of Charlier moments, by using less mathematical operations of the image pixels is achieved by describing an image with a set of blocks instead of individual pixels. The computation of Charlier moments can be accelerated by using the methodology of the image block representation [15].

In the following two subsections, we will propose a new formula to fast compute the discrete orthogonal Charlier moments in the image blocks representation for binary and gray-scale images.

3.1 For Binary Images

In order to accelerate the time computation of Charlier moments we will apply the algorithm of image block representation (IBR) [15]. In this approach, the binary image is represented as a set of blocks, each block corresponding to an object. This block is defined as a rectangular area that includes a set of connected pixels. By applying the IBR algorithm, the binary image is described by the relation:

$$f(x,y)=\{b_i, i=0,1,....,K-1\} \tag{20}$$

where b_i is the ith block and K is the total number of blocks. Each block is described by the coordinates of the upper left and down right corner in vertical and horizontal axes. The Eq. (19) can be rewritten as

$$CM_{nm}=\sum_{i=0}^{k-1}\sum_{x=x_{1,b_i}}^{x_{2,b_i}}\sum_{y=y_{1,b_i}}^{y_{2,b_i}}\tilde{C}_n^{a_1}(x)\tilde{C}_m^{a_1}(y)=\sum_{i=0}^{k-1}CM_{nm}^{b_i} \tag{21}$$

with (x_{1,b_i}, x_{2,b_i}) and (y_{1,b_i}, y_{2,b_i}) are respectively the coordinates in the upper left and lower right block b_i, and $CM_{nm}^{b_i}$ the moment the block b_i is given by:

$$\begin{aligned} CM_{nm}^{b_i} &= \sum_{x=x_{1,b_i}}^{x_{2,b_i}}\sum_{y=y_{1,b_i}}^{y_{1,b_i}}\tilde{C}_n^{a_1}(x)\tilde{C}_m^{a_1}(y) \\ &= \sum_{x=x_{1,b_i}}^{x_{2,b_i}}\tilde{C}_n^{a_1}(x)\sum_{y=y_{1,b_i}}^{y_{2,b_i}}\tilde{C}_m^{a_1}(y) \\ &= S_n(x_{1,b_i}, x_{2,b_i})S_m\left(y_{1,b_i}, y_{2,b_i}\right) \end{aligned} \tag{22}$$

with

$$S_n(x_{1,b_i}, x_{2,b_i})=\sum_{x=x_{1,b_i}}^{x_{2,b_i}}\tilde{C}_n^{a_1}(x) \quad \text{and} \quad S_m(y_{1,b_i}, y_{2,b_i})=\sum_{y=y_{1,b_i}}^{y_{2,b_i}}\tilde{C}_m^{a_1}(y) \tag{23}$$

3.2 For Gray-Scale Images

The approach of intensity slice representation (ISR) decomposes an image gray-scale $f(x,y)$ in series of slices

$$f(x,y)=\sum_{i=1}^{L}f_i(x,y) \tag{24}$$

where L is the number of slices and f_i the intensity function of the ith slice

After the decomposition of gray scale image into several slices of two levels, we can apply the algorithm ISR [19]. The gray-scale image $f(x,y)$ can be redefined in terms of blocks of different intensities.

$$\begin{aligned} f(x,y) &= \{f_i(x,y), i=1,2,....,L\} \\ f_i(x,y) &= \{b_{ij}, j=1,2,....,K_i-1\} \end{aligned} \tag{25}$$

where b_{ij} is the block of the edge i and K_i is the number of image blocks with intensity.

The fast computation of Charlier moments for gray-scale image $f(x,y)$ is given by

$$\begin{aligned} CM_{nm} &= \sum_{x=0}^{N-1}\sum_{y=O}^{N-1}\tilde{C}_n^{a_1}(x)\tilde{C}_m^{a_1}(y)\sum_{i=1}^{L}f_i(x,y) \\ &= \sum_{i=1}^{L}\sum_{x=0}^{N-1}\sum_{y=O}^{N-1}\tilde{C}_n^{a_1}(x)\tilde{C}_m^{a_1}(y)f_i(x,y) \\ &= \sum_{i=1}^{L}f_iM_{nm}(i) \end{aligned} \tag{26}$$

where $M_{nm}(i)$ are the (n+m) order Charlier moments of the i[th] binary slice.

4 Images Reconstruction Using Charlier Moments

In this section, the image representation capability of Charlier moments is shown. The Charlier moments of the image are first calculated and subsequently its image representation power is verified by reconstructing the image from the moments. An objective measure based on mean squared error (MSE) is used to characterize the error between the original image and the reconstructed image. Indeed, The Charlier moments of order (n+m) in terms of Charlier normalized discrete orthogonal polynomials, for an image with intensity function, $f(x,y)$, is defined as

$$CM_{nm} = \sum_{x=0}^{M-1}\sum_{y=0}^{N-1} \tilde{C}_n^{a_1}(x)\tilde{C}_m^{a_1}(y)\, f(x,y) \tag{27}$$

By solving the equatios Eq (6) and Eq (19) the image intensity function $f(x,y)$ can be written completely in terms of the Charlier moments as

$$f(x,y) = \sum_{n=0}^{N-1}\sum_{m=0}^{N-1} CM_{nm}\tilde{C}_n^{a_1}(x)\tilde{C}_m^{a_1}(y) \tag{28}$$

The image intensity function can be represented as a series of normalized Charlier polynomials weighted by the Charlier moments. If the moments are limited to order max, the series is truncated to

$$\hat{f}(x,y) = \sum_{n=0}^{\max}\sum_{m=0}^{n} CM_{n-m,m}\tilde{C}_n^{a_1}(x)\tilde{C}_m^{a_1}(y) \tag{29}$$

The difference between the original image $f(x,y)$ and the reconstructed images $\hat{f}(x,y)$ is measured using the mean squared error (MSE) defined as follows

$$MSE = \frac{1}{MN}\sum_{i=1}^{M}\sum_{j=1}^{N}\left(f(x_i,y_j) - \hat{f}(x_i,y_j)\right)^2 \tag{30}$$

5 Charlier's Invariant Moments

To use the Charlier moments for the object classification, it is indispensable that Charlier invariant moments be under rotation, scaling, and translation of the image. Therefore to obtain the translation, scale and rotation invariants of Charlier moments, we adopt the same strategy used by Papakostas et al. for Krawtchouk moments [28]. That is, we derive the Charlier's invariant moments through the geometric moments using the conventional method and the fast method based on image block representation.

5.1 Computation of Charlier's invariant moments

Given a digital image $f(x,y)$ with size N×N, the geometric moments $f(x,y)$ is defined using discrete sum approximation as:

$$GM_{nm} = \sum_{x=0}^{N-1}\sum_{y=0}^{N-1} x^n y^m f(x,y) \tag{31}$$

The set of geometric moment invariant by rotation, scaling and translation can be written as [1]

$$GMI_{nm} = GM_{00}^{-\gamma}\sum_{x=0}^{N-1}\sum_{y=0}^{N-1}\left[(x-\bar{x})\cos\theta + (y-\bar{y})\sin\theta\right]^n \times\left[(y-\bar{y})\cos\theta - (x-\bar{x})\sin\theta\right]^m f(x,y) \tag{32}$$

with

$$\bar{x} = \frac{MG_{10}}{MG_{00}}\ ;\ \bar{y} = \frac{MG_{01}}{MG_{00}}$$
$$\gamma = \frac{n+m}{2}+1\ ;\ \theta = \frac{1}{2}\tan^{-1}\frac{2\mu_{11}}{\mu_{20}-\mu_{02}} \tag{33}$$

The (n+m)th central geometric moments is defined in [1] by

$$\mu_{nm} = \int_{-\infty}^{\infty}\int_{-\infty}^{\infty}(x-\bar{x})^n(y-\bar{y})^m f(x,y)dxdy \tag{34}$$

This formula can be approximated by

$$\mu_{nm} = \sum_{x=0}^{N-1}\sum_{y=0}^{M-1}(x-\bar{x})^n(y-\bar{y})^m f(x,y) \tag{35}$$

The Charlier moment invariants can be expanded in terms of GMI Eq. (2) as follows

$$CMI_{nm} = \sum_{i=0}^{n}\sum_{j=0}^{m}\alpha_{i,n}^{a_1}\alpha_{j,m}^{a_1}V_{i,j} \tag{36}$$

where $a_{i,j}^{a_1}$ are the coefficients relative to Eq. (1) and $V_{i,j}$ are the parameters defined as

$$V_{nm} = \sum_{q=0}^{n}\sum_{p=0}^{m}\binom{n}{p}\binom{m}{q}\left(\frac{N\times M}{2}\right)^{((p+q)/2)+1}\left(\frac{N}{2}\right)^{n-p}\left(\frac{M}{2}\right)^{m-p} GMI_{pq} \tag{37}$$

5.2 Fast computation of Charlier's invariant moments

In order to accelerate the time computation of Charlier's invariants moments, we will applied the algorithms of image block representation described previously.

By using the binomial theorem, the GMI defined in Eq. (32) can be calculated as follows:

$$GMI_{nm} = GM_{00}^{-\gamma}\sum_{i=0}^{n}\sum_{j=0}^{m}\binom{n}{i}\binom{m}{j}(\cos\theta)^{i+j}(\sin\theta)^{n+m-i-j} \times(-1)^{m-j}\mu_{m+i-j,n+j-i} = \sum_{i=0}^{n}\sum_{j=0}^{m}\binom{n}{i}\binom{m}{j}(\cos\theta)^{i+j}(\sin\theta)^{n+m-i-j} \times(-1)^{m-j}\eta_{m+i-j,n+j-i} \quad (38)$$

where

$$\eta_{nm} = \frac{\mu_{nm}}{GM_{00}^{\gamma}} \quad (39)$$

By applying the algorithm IBR, the normalized central moment defined in Eq. (35) can be calculated as follows

$$\begin{aligned}\eta_{nm} &= \frac{\mu_{nm}}{GM_{00}^{\gamma}} = \frac{1}{GM_{00}^{\gamma}}\sum_{x=0}^{N-1}\sum_{y=0}^{M-1}(x-\bar{x})^n(y-\bar{y})^m f(x,y)\\ &= \frac{1}{GM_{00}^{\gamma}}\sum_{x=0}^{N-1}\sum_{y=0}^{M-1}(x-\bar{x})^n(y-\bar{y})^m(\sum_{k=1}^{S} f_k(x,y))\\ &= \frac{1}{GM_{00}^{\gamma}}\sum_{k=1}^{S} f_k \times \sum_{x=0}^{N-1}\sum_{y=0}^{M-1}(x-\bar{x})^n(y-\bar{y})^m\\ &= \frac{1}{GM_{00}^{\gamma}}\sum_{k=1}^{S} f_k \times \sum_{j=0}^{k}\left[\left(\sum_{x_k=x_{1,b_j}}^{x_{2,b_j}}(x-\bar{x})^n\right)\left(\sum_{y_k=y_{1,b_j}}^{y_{2,b_j}}(y-\bar{y})^m\right)\right]\\ &= \frac{1}{GM_{00}^{\gamma}}\sum_{k=1}^{S} f_k \times \eta_{nm}^{k}\end{aligned} \quad (40)$$

where

$$\eta_{nm}^{k} = \sum_{j=0}^{k}\left[\left(\sum_{x_k=x_{1,b_j}}^{x_{2,b_j}}(x-\bar{x})^n\right)\left(\sum_{y_k=y_{1,b_j}}^{y_{2,b_j}}(y-\bar{y})^m\right)\right] \quad (41)$$

and f_k ; k=1,2,.....S is the slices intensity functions, S is the number of slices in image f , b_j ; j=1,2,....k is the block in each slice. (x_{1,b_i}, y_{1,b_i}) and (x_{2,b_i}, y_{2,b_i}) are respectively the coordinates in the upper left and lower right block b_j Using the previous equations Eq. (38) and Eq. (40), the GMI of Eq. (32) can be rewritten as:

$$\begin{aligned}GMI_{nm} &= \sum_{i=0}^{n}\sum_{j=0}^{m}\binom{n}{i}\binom{m}{j}(\cos\theta)^{i+j}(\sin\theta)^{n+m-i-j}\times(-1)^{m-j}\eta_{m+i-j,n+j-i}\\ &= \frac{1}{GM_{00}^{\gamma}}\sum_{i=0}^{n}\sum_{j=0}^{m}\binom{n}{i}\binom{m}{j}(\cos\theta)^{i+j}(\sin\theta)^{n+m-i-j}\times(-1)^{m-j}\sum_{k=1}^{S} f_k\times\eta_{m+i-j,n+j-i}^{k}\\ &= \frac{1}{GM_{00}^{\gamma}}\sum_{k=1}^{S} f_k\sum_{i=0}^{n}\sum_{j=0}^{m}\binom{n}{i}\binom{m}{j}(\cos\theta)^{i+j}(\sin\theta)^{n+m-i-j}\times(-1)^{m-j}\times\eta_{m+i-j,n+j-i}^{k}\end{aligned} \quad (42)$$

Therefore the Charlier moments invariant under translation, scaling and rotation can be obtained from the equations Eq. (36), Eq. (37) and Eq. (42).

6 Results and Simulations

In this section, we give experimental results to validate the theoretical results developed in the previous sections. This section is divided into foursub-sections. In the first sub-section, we will compare the time computation of Charlier's moments by direct method and proposed method for binary and gray-scale images. In the second one, we will test the ability of Charlier's moments for the reconstruction of binary and gray-scale images with and without noise. In sub-section three, the invariability of Charlier moments under the three transformations translation, scaling and rotation is shown. In the last sub-section, the recognition accuracy of Charlier's invariant moments is tested a compared to that of Hu's and Legendre's invariant moment in object recognition.

6.1 The computational time of Charlier's moments

In this sub-section, we will compare the computational time of Charlier's moments by two methods: the direct method based on Eq. (11) and Eq. (19) and the proposed fast method based on the use of recurrence relation with respect to the variable x defined by Eq. (17) and the application of image block representation methodology defined previously by Eq. (22) and Eq. (26).

In the first example, a set of five binary images with size 200x200 pixels (Fig.1) selected from craft patterns handwritten were used as test images. The number of blocks of these images is NB=1450 for image (a), NB=1428 for image (b), NB=2107 for image (c), NB=2324 for image (d), and NB=2854 for image (e). The computational processes are performed 20 times for each of the five images

(a) (b) (c) (d) (e)

Fig.1. Set of test binary images

where the average times are plotted (Fig.2) against the moment order for the images above using the proposed method and the direct method. Fig.2 shows that our proposed method is faster than the direct method. Note that the computation time for extracting the blocks of each image is about 1ms, this time is much less than the computation time required in the calculation of moments.

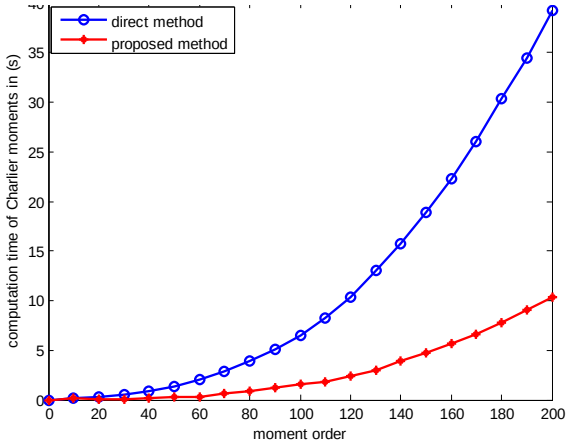

Fig. 2. Average computation time for binary images using direct method and our method.

In the second example, a set of five gray-scale images with a size of 128x128 pixels, shown in Fig.3, are used. The number of blocks and slices of these images are NB=14106, NS=200 for Lena, NB= 14384; NS=251 for Highway, NB=12491; NS= 243 for Lake, NB=14016; NS=223 for Pepper and NB=15359; NS=194 for Mandrill. The computation time to extract the blocks of each image is about 1ms. The computational processes are performed 19 times for each of the five images. The average times are plotted against the moment order in Fig. 4. The result indicates again that our method has a better performance than the direct method. Note that the algorithm was implemented on a PC Dual Core 2.10 GHz, 2GB of RAM.

(a) (b) (c) (d) (e)

Fig. 3. Set of test gray-scale images (a) Lena, (b) Highway, (c) Lake, (d) Pepper and (e) Mandrill

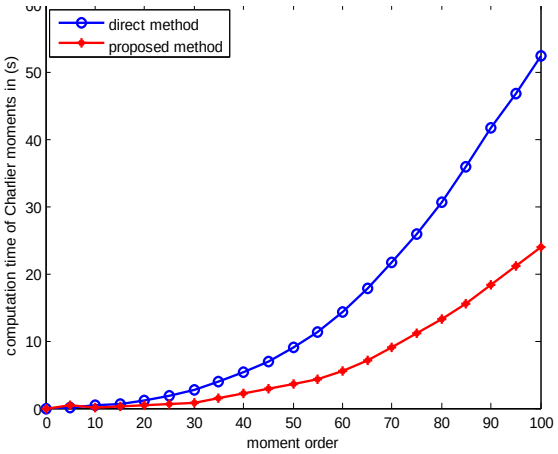

Fig. 4. Average computation time for gray-scale images using direct method and proposed method.

The two figures show that the proposed method is faster than the direct method because the computation of Charlier's moments by fast method depends only on the number of blocks than the image's size.

6.2 Image Reconstruction using Charlier's Moment

In this section we will discuss the ability of Charlier's moments for the reconstruction of the binary and gray-scale images using the proposed method. To evaluate this method, we will calculate the mean squared error (MSE) defined by Eq. (30) between the original and the reconstructed image. MSE is largely used in the domain of image analysis as a quantitative measure of accuracy.

Two numerical experiments have been carried out to verify the image reconstruction capability of the proposed method when they are used for gray-level image or binary image. The test of both binary image "Zewaka: image (a)" of size 200x200 (Fig. 1) is used with a maximum moment order ranging from 0 to 200 and the gray-scale image "Highway" of size 128×128 (Fig. 2) is used with a maximum moment order ranging from 0 to 100. Fig. 6 and Fig. 7 show the MSE of the proposed method. It is obvious that the MSE decreases as the moment of order increases where the MSE gets near to zero with increasing moment order. When the maximum moment order gets to a certain value, the reconstructed images will be very close to the original ones.

To show the robustness of the proposed Charlier's moments against the negative effects of different types of noise, two numerical experiments are performed for the two previous images using two types of noises. The images contaminated with a first type of noise "salt and pepper" and with the second type of noise "white Gaussian" noise'' are shown in Fig. 5. The four contaminated images are reconstructed using the proposed Charlier moments. The plotted curves of MSE for the noise contaminated images are displayed in Fig.6 and Fig.7. For easier comparison, the two curves of MSE are plotted in the same figure. Generally, the MSE of noisy images is greater than the corresponding values of MSE without image noise. All figure shows the curves of the noise contaminated image MSE approaches zero while increasing the moments order. The results of these experiments show the robustness of Charlier moments against different types of noise.

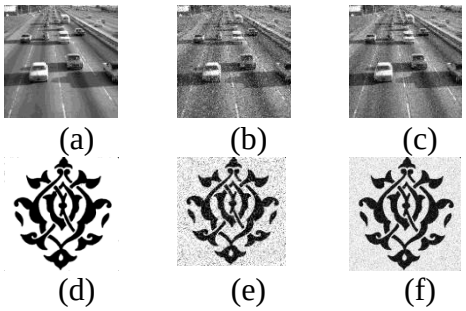

Fig. 5. Set of noisy images. (a) Highway gray-scale image, (b) noisy by Salt & Peppers and (c) noisy image by white Gaussian, (d) Zewaka binary image, (e) noisy by Salt & Peppers and (f) noisy image by white Gaussian,

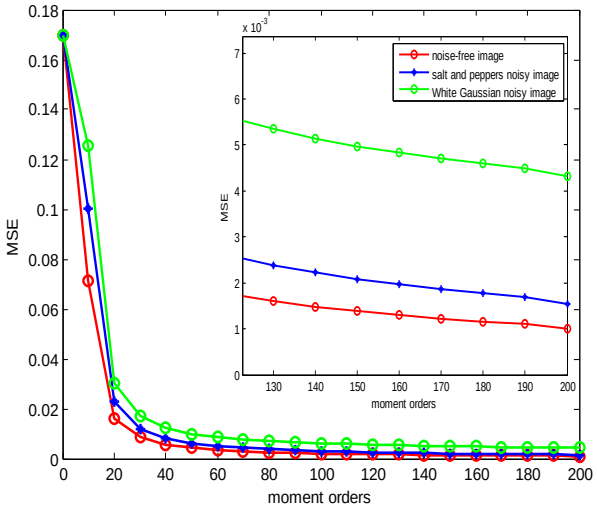

Fig. 6. Comparative study of reconstruction error MSE for binary image of "Zewaka" with salt & peppers and white Gaussian noise versus order Charlier moments.

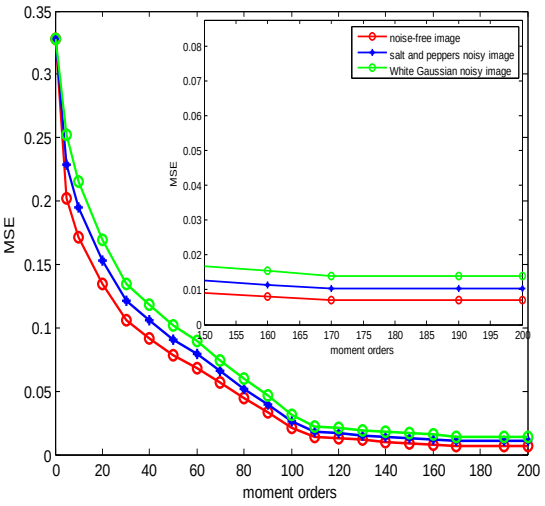

Fig. 7. Comparative study of reconstruction error MSE for gray-scale image of "Highway" with salt & peppers and white Gaussian noise versus order Charlier moments.

6.3 Invariability

The binary image "image (a)" whose size is 128x128 pixels displayed in Fig.1 is used in order to evaluate the property of invariability of the proposed Charlier's invariant moments. This image is scaled by a factor varying from 0.1 to 2 with interval 0.05, rotated from 00 to 1800 with interval 100 and translated by a vectors varying from (-5,-5) to (5,5). Each translation vector consists of two elements which represent a vertical and a horizontal image shift respectively. These three image transformations and a combination of them are applied on the dataset which is created by the transformed images (Fig. 8).

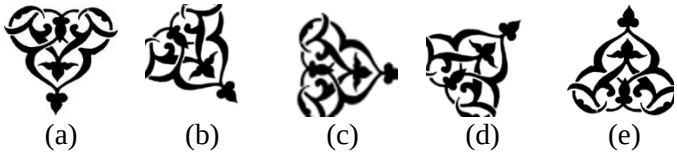

Fig. 8. Set of mixed transformed binary image Zewaka

All invariant moments of Charlier is calculated up to order two for each transformation. Finally, in order to measure the ability of the proposed moment invariants of Charlier to remain unchanged under different image transformations, We define the relative error between the two sets of moment invariants corresponding to the original image *f(x,y)* and the transformed image *g(x,y)* as

$$E_{CM}(f,g)=\frac{\|CMI(f)-CMI(g)\|}{\|CMI(f)\|} \tag{43}$$

where $\|.\|$ denotes the Euclidean norm and $CMI(f)$; $CMI(g)$ are the Charlier's invariant moments for the original image f and the transformed image g . The results are plotted in Figures (9, 10 and 11) for the case $(a_1=60)$.

Fig. 9 compares the relative errors between the proposed method and the Hu's invariant moments [1]. It can be seen from this figure that the Charlier's moment invariants shows better performance than the Hu's invariant moments, whatever the rotational angle.

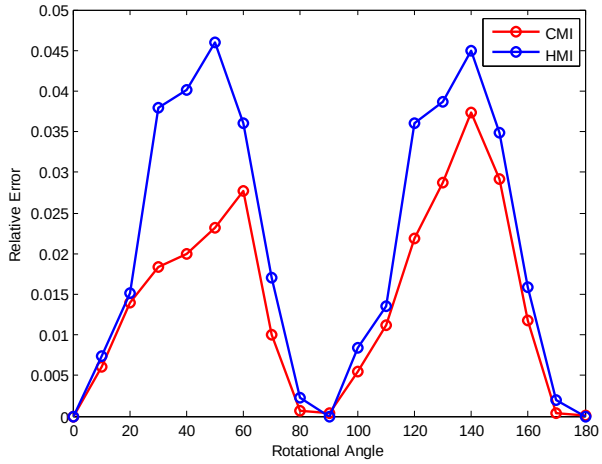

Fig. 9. Performance of the Charlier and Hu invariant moments to rotation. Horizontal axis: rotational angle; vertical axis: relative error between the rotated image and the original image.

Fig. 10 shows the relative error of the charlier's invariant moments and the geometric invariant of Hu. Plots show that, in most cases, the relative errors of Charlier invariant moments is lower than the geometric invariant moments, whatever the scaling factor.

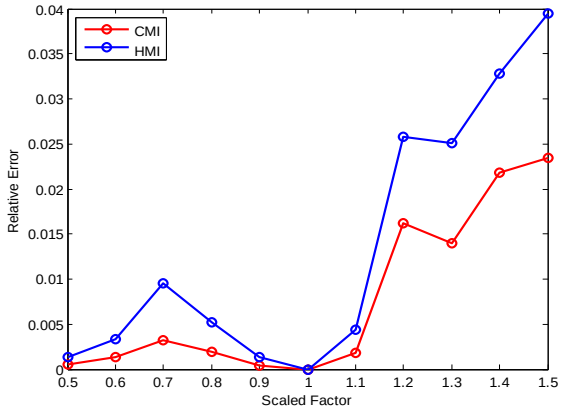

Fig. 10. Performance of the Charlier and Hu invariant moments to scale. Horizontal axis: scaled factor; vertical axis: relative error between the rotated image and the original image.

Fig. 11 shows the relative error of the charlier's invariant moments and the geometric invariant of Hu. Plots show that, in most cases, the relative errors of Charlier invariant moments is lower than the geometric invariant moments, whatever the translation vectors.

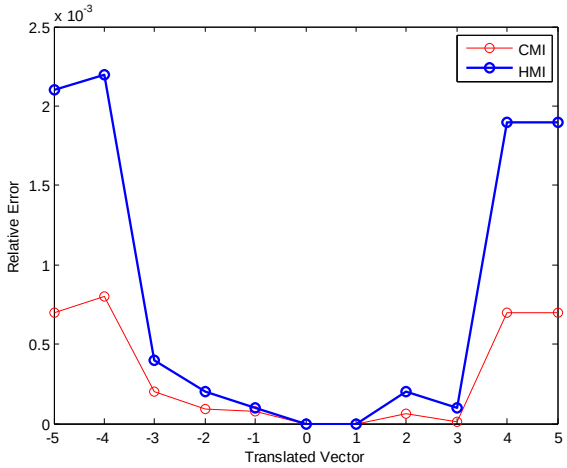

Fig. 11. Performance of the Charlier and Hu invariant moments to translation. Horizontal axis: scaled factor; vertical axis: relative error between the rotated image and the original image.

To test the robustness to noise, we have respectively added a white Gaussian noise (with mean $\mu = 0$ and different variances) and salt-and-pepper noise (with different noise densities). Results are respectively depicted in Figs. 12 and 13. It can be seen that, if the relative error increases with the noise level, the proposed descriptors are more robust to noise than the geometric invariants of Hu.

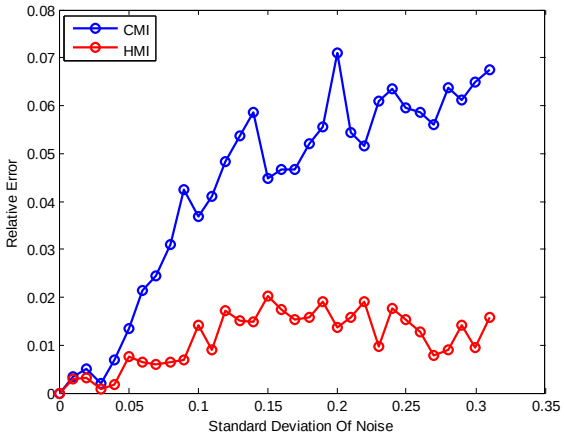

Fig. 12. Performance of the Charlier and hu invariant moments with respect to additive Gaussian zero-mean random noise. Horizontal axis: standard deviation of noise; vertical axis: relative error between the corrupted image and original image.

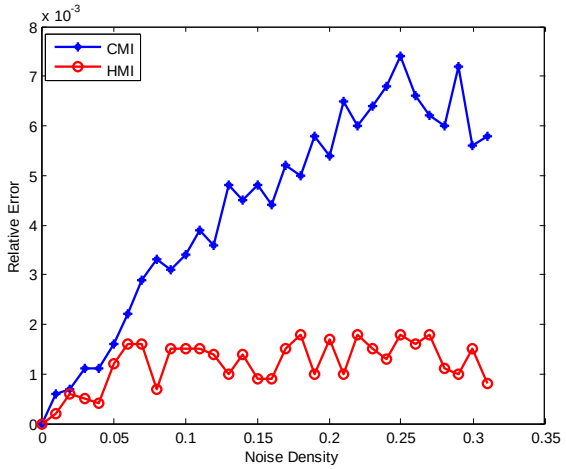

Fig. 13. Performance of the Chrlier and Hu invariant moments with respect to additive salt-and-pepper noise. Horizontal axis: noise density; vertical axis: relative error between the corrupted image and original image

It is clear from the figures that the relative error is very low, indicating that the Charlier's invariant moments are very stable under different types of image transformations and different types of noises which give excellent results with Charlier's invariants moment. Therefore, the invariants moments derived in this paper could be a useful tool in pattern recognition tasks that require the translation, scaling and rotation invariance.

6.4 Classification

In this section we will provide experiences to validate the precision of recognition and the classification of objects using the proposed Charlier's invariants moments. For this, we will put in place the characteristic vectors defined by:

$$V=[CMI_{ij}] \quad ; \quad 0\le i,j\le 2 \tag{44}$$

where $V=[CMI_{ij}] \quad ; \quad 0\le i,j\le 2$ are the Charlier moment invariants defined in Section 5.

To perform the classification of the objects to their appropriate classes we will use simple classifiers based on plain distances. The Euclidean distance is utilized as the classification measure [34].

$$d(x_s,x_t^{(k)})=\sqrt{\sum_{j=1}^{n}(x_{sj}-x_{tj}^{(k)})^2} \tag{45}$$

The above formulas measure the distance between two vectors where x_s is the n -dimensional feature vector of unknown sample, and $x_t^{(k)}$ the training vector of class k. If the two vectors x and y are equals, then d tend to 0. Therefore to classify the images, one takes the minimum values of the distance.

We define the recognition accuracy as:

$$\eta=\frac{\text{Number of correctly classified images}}{\text{The total of images used in the test}}\times 100\% \tag{46}$$

In order, to validate the precision of recognition and the classification of objects using the proposed Charlier's invariant moments, we well use two image databases. The first database is the Columbia Object Image Library (COIL-20) database [35]. The reason for choosing such a set is that the objects (three toy cars, three blocks, ANACIN and TYLENOL packs) can be easily misclassified due to their similarity. Each image is resized in 128x128. This base has the characteristic of being widely used in image classification. An overview of this database is presented in Fig.14. The total number of images is 1440 distributed as 72 images for each object. This is followed by adding salt-and-pepper noise with different noise densities.

The second image database is formed by a set of

Fig. 14. Collection of the COIL-20 object.

craft patterns handwritten whose size is 100x100 pixels shown in Fig1. The images are transformed by translating; scaling and rotating the original set with translation $TV=\{(-5,-5);(-5,0);(-5,5);(0,0);(0,-5);(0,5);(5,-5);(5,0);(5,5)\}$ in horizontal and vertical directions, scale factor $SF\in\{1.2,\ 1.1,1,0.9,\ 0.8\}$ and rotation angle $\theta\in\{0^0,45^0,90^0,135^0,180^0,225^0,270^0,315^0\}$ forming a set of 1800 images. A salt-and pepper noise with different noise densities has been added. The feature vector based on Charlier's moment invariants cited in Eq. (42) are used to classify these images and its recognition accuracy is compared with that of Hu's moment invariants [1] and Legendre moment invariants [31] for the two databases. The classification results of two databases are presented in Tables (1.1 and 1.2) respectively. The results show the efficiency of the proposed Charlier's

invariant moments in terms of recognition accuracy of noisy images, compared to those of Hu and Legendre. Note that the recognition of non-noisy image by our method is 100% and the accuracy of the recognition decreases with increasing noise. Finally, the proposed Charlier's moment invariants are robust to image transformations under noisy conditions, and the recognition accuracy of which are better than that of Hu's and Legendre's moment invariants.

TABLE1.2
Classification results of COILL-20 objects database using euclidean distance

		Salt &pepper noise			
	Noise free	1%	2%	3%	4%
Hu	96.56%	93.28%	84.12%	75.23%	70.68%
Legendre	97.25%	95.08%	86.83%	76.47%	74.24%
Charlier	97.52%	95.56%	88.94%	81.36%	75.25%

TABLE1.1
Classification results of craft patterns handwritten database using euclidean distance

		Salt &pepper noise			
	Noise free	1%	2%	3%	4%
Hu	100%	95.5%	87.23%	77.66%	73.65%
Legendre	100%	96.76%	92.52%	91.65%	90.47%
Charlier	100%	97.32%	95.26%	92.05%	91.23%

7 Conclusion

In this paper, we have proposed a new fast method for the computation of a new set of Charlier's discrete orthogonal moments for binary and gray-scale images. This new fast method is performed using some properties of Charlier's discrete orthogonal polynomials and the image block representation. The computation of Charlier's moments, using this method, eliminates the propagation of numerical error and depends only on the number of blocks, which can significantly reduce the time computation of Charlier's moments. The effectiveness of the proposed Charlier's moments for the reconstruction of binary and gray-scale images with noise and without noise has been showed by experimental results. Furthermore, we have proposed a new set of Charlier's invariant moments. The accuracy of recognition of the proposed Charlier's invariant moments in the object classification related to Hu's and Legendre's invariant moments is carried out.

References:

[1] M. K. Hu, "Visual Pattern Recognition By Moment Invariants," IRE Trans. Inform. Theory, Vol. It-8, Pp. 179–187, Feb. 1962.

[2] S.A. Dudani, K.J. Breeding, and R.B. Mcghee, "Aircraft Identification by Moment Invariant" IEEE Trans. Comput., Vol. 26, No. 1, pp. 39-46, 1977.

[3] J. Flusser, "Pattern Recognition by Affine Moment Invariants," Pattern Recognition, Vol. 26, No. 1, Pp. 167-174, 1993.

[4] M.R. Teague, "Image Analysis via The General Theory Of Moments," J. Opt. Soc. Amer. Vol. 70, pp. 920–930 , 1980.

[5] C.-W. Chong, R. Paramesran, and R. Mukundan, "Translation and Scale Invariants of Legendre Moments," Pattern Recognition, vol. 37, no. 1, pp. 119-129, 2004.

[6] A. Khotanzad, Y.H. Hong, "Invariant Image Recognition by Zernike Moments", IEEE Transactions on Pattern Analysis and Machine Intelligence, Vol. 12, pp 489–497, 1990.

[7] Y.L. Sheng, L.X. Shen, Orthogonal Fourier–Mellin moments for invariant pattern recognition, Journal Optical Society America 11 (1994) 1748–1757.

[8] C.H. Teh, R.T. Chin, "On Image Analysis by the Method of Moments", IEEE Trans. Pattern Anal. Mach. Intell., Vol. 10, No.4, pp. 496–513, 1988.

[9] S.X. Liao, M. Pawlak, "On Image Analysis by Moments," IEEE Trans. Pattern Anal.Mach. Intell, Vol. 18, No. 3, pp. 254–266, 1996.

[10] R. Mukundan, S.H. Ong, and P.A. Lee, "Image Analysis By Tchebichef Moments," IEEE Trans. Image Process., vol. 10, no. 9, pp. 1357-1364, 2001.

[11] P.T. Yap, R. Paramesran, S.H. Ong, "Image analysis by Krawtchouk moments," IEEE Transactions on Image Processing, Vol. 12,.No. 11, pp. 1367–1377, 2003.

[12] P.T. Yap, P. Raveendran, and S.H. Ong, "Image Analysis Using Hahn Moments," IEEE Trans. Pattern Anal. Mach. Intell., vol. 29, no. 11, pp. 2057-2062, 2007.

[13] R. Mukundan, "Some Computational Aspects of Discrete Orthonormal Moments," IEEE Transactions on Image Processing, Vol. 13, No. 8, pp. 1055–1059, 2004.

[14] H. Zhu, M. Liu, H. Shu, H. Zhang and L. Luo," General Form For Obtaining Discrete Orthogonal Moments,'' IET Image Process., Vol. 4, Iss. 5, pp. 335–352 335 October 2010.

[15] I.M. Spiliotis and B.G. Mertzios, "Real-Time Computation of Two-Dimensional Moments

On Binary Images Using Image Block Representation," IEEE Trans. Image Process, vol. 7, no. 11, pp. 1609-1615, 1998.

[16] G.A. Papakostas, E.G. Karakasis, D.E. Koulouriotis," Accurate and Speedy Computation Of Image Legendre Moments For Computer Vision Applications", Image and Vision Computing, Vol 28, Issue 3, Pages 414-423, March 2010.

[17] J. Flusser, "Refined Moment Calculation Using Image Block Representation," IEEE Transactions on Image Processing, vol.9, no.11, pp.1977-1978, Nov 2000.

[18] H.Z. Shu, H. Zhang, B. J. Chen, P. Haigron, and L.M. Luo,"Fast Computation Of Tchebichef Moments for Binary and Gray-Scale Images,"IEEE Transactions on Image Processing, vol.19, no.12, pp.3171-3180, Dec. 2010.

[19] G.A. Papakostas, E.G. Karakasis, and D.E. Koulourisotis, "Efficient and Accurate Computation of Geometric Moments on Gray-Scale Images," Pattern Recognit, vol. 41, no. 6, pp. 1895-1904, 2008.

[20] K.M. Hosny, "Exact and Fast Computation of Geometric Moments for Gray Level Images", Appl. Math. Comput., vol 189, pp. 1214–1222, 2007.

[21] G.A. Papakostas, E.G. Karakasis, and D.E. Koulourisotis, "A Unified Methodology for Efficient Computation of Discrete Orthogonal Image Moments," Information Sciences, vol. 179, no. 20, pp. 3619-3633, 2009.

[22] M. Sayyouri ,A. Hmimd , H. Qjidaa, " A Fast Computation of Charlier Moments for Binary and Gray-Scale Images,"The 2nd edition of the IEEE Colloquium on Information Sciences and Technology (CIST'12), Fez, Morocco, 22-24 October 2012.

[23] B. Bayraktar, T. Bernas, J.P. Robinson, and B. Rajwa, "A Numerical Recipe for Accurate Image Reconstruction from Discrete Orthogonal Moments," Pattern Recognit, vol. 40, no. 2, pp. 659-669, 2007.

[24] M. Sayyouri, A. Hmimd, H. Qjidaa" A Fast Computation of Hahn Moments for Binary and Gray-Scale Images "IEEE .International Conference on Complex Systems ICCS'12, Agadir, Morocco, 5 & 6 November -2012.

[25] C.-W. Chong, P. Raveendran, R. Mukundan," Translation Invariants of Zernike Moments," Pattern Recognition, Vol. 36, pp. 1765–1773, 2003.

[26] C.-W. Chong, P. Raveendran, R. Mukundan, "Translation and Scale invariants of Legendre Moments," Pattern Recognition, Vol. 37, pp. 119–129, 2004.

[27] H. Zhu, H. Shu, T.Xia, L. Luo, J. L. Coatrieux," Translation and Scale Invariants of Tchebichef Moments", Pattern Recognition, Vol 40, Issue 9, pp 2530-2542, September 2007.

[28] G.A. Papakostas, E.G. Karakasis, D.E. Koulouriotis, "Novel Moment Invariants for Improved Classification Performance In Computer Vision Applications," Pattern Recognition, Vol 43, Issue 1, pp. 58-68, January 2010.

[29] H. Zhu, H. Shu, J. Zhou, L.Luo, J.L. Coatrieux, "Image Analysis by Discrete Orthogonal Dual Hahn Moments", Pattern Recognition Letters, Vol 28, Iss 13, pp 1688-1704, 1 October 2007, .

[30] E.G. Karakasis, G.A. Papakostas, D.E. Koulouriotis, V.D. Tourassis ,"Generalized Dual Hahn Moment Invariants", Pattern Recognition, Vol 46, Iss 7, Pages 1998-2014, July 2013.

[31] H. Zhang, H.Z. Shu,G.N. Han, G.Coatrieux, L.M. Luo; J.L. Coatrieux, "Blurred Image Recognition by Legendre Moment Invariants", IEEE Transactions Image Processing, Image Processing Vol.19, no.3, pp.596,611, March 2010.

[32] A.F.Nikiforov, S.K. Suslov, B. Uvarov, "Classical Orthogonal Polynomials of A Discrete Variable," (Springer, New York, 1991).

[33] R. Koekoek, P.A.Lesky and R.F. Swarttouw "Hypergeometric Orthogonal Polynomials and Their Q-Analogues". Springer Monographs in Mathematics. Library of Congress Control Number: 2010923797.

[34] R. Mukundan, K.R. Ramakrishnan,"Moment Functions in Image Analysis," World Scientific Publisher, Singapore, 1998.

[35] http://www.cs.columbia.edu/CAVE/software/softlib/coil-20.php